Research Article | Vol. 26, No. 13 | 25 Jun 2018 | OPTICS EXPRESS 16074
Optics EXPRESS

10 W CEP-stable few-cycle source at 2 μm with 100 kHz repetition rate

M. Neuhaus,[1] H. Fuest,[1,2] M. Seeger,[1,2] J. Schötz,[1,2] M. Trubetskov,[2] P. Russbueldt,[3] H.D. Hoffmann,[3] E. Riedle,[4] Zs. Major,[1,2] V. Pervak,[1] M. F. Kling,[1,2,6] and P. Wnuk[1,2,5,7]

[1]*Physics Department, Ludwig-Maximilians-Universität Munich, Am Coulombwall 1, D-85748 Garching, Germany*
[2]*Max Planck Institute of Quantum Optics, Hans-Kopfermann-Straße 1, D-85748 Garching, Germany*
[3]*Fraunhofer Institute for Laser Technology, Steinbachstr. 15, D-52074 Aachen, Germany*
[4]*Lehrstuhl für BioMolekulare Optik, Ludwig-Maximilians-Universität München, Oettingenstrasse 67, D-80538 München, Germany*
[5]*Institute of Physical Chemistry, Polish Academy of Sciences, Kasprzaka 44/52, 01-224 Warsaw, Poland*
[6]*matthias.kling@lmu.de*
[7]*pwnuk@mpq.mpg.de*

Abstract: We developed a high repetition rate optical parametric chirped-pulse amplification (OPCPA) laser system based on fiber-laser-seeded Innoslab to generate few-cycle pulses around 2 μm with passively stable carrier-envelope phase (CEP) by difference frequency generation (DFG). Incorporating a piezo mirror before the DFG stage permits rapid CEP control. The OPCPA system is seeded by a stable supercontinuum generated in bulk material with the picosecond Innoslab pulses. Few-cycle pulses with durations of 17 fs and energies of over 100 μJ were produced in a single OPCPA stage. Three different nonlinear crystals: BBO, BiBO, and LNB were tested in the final parametric amplifier, and their average power related limitations are addressed.

OCIS codes: (140.3070) Infrared and far-infrared lasers; (140.7090) Ultrafast lasers; (190.4970) Parametric oscillators and amplifiers; (190.7110) Ultrafast nonlinear optics; (320.7090) Ultrafast lasers; (320.7110) Ultrafast nonlinear optics.

References and links

1. M. F. Kling, P. von den Hoff, I. Znakovskaya, and R. de Vivie-Riedle, "(Sub-)femtosecond control of molecular reactions via tailoring the electric field of light," Phys. Chem. Chem. Phys. **15**(24), 9448–9467 (2013).
2. F. Krausz and M. Ivanov, "Attosecond physics," Rev. Mod. Phys. **81**(1), 163–234 (2009).
3. B. Förg, J. Schötz, F. Süßmann, M. Förster, M. Krüger, B. Ahn, W. A. Okell, K. Wintersperger, S. Zherebtsov, A. Guggenmos, V. Pervak, A. Kessel, S. A. Trushin, A. M. Azzeer, M. I. Stockman, D. Kim, F. Krausz, P. Hommelhoff, and M. F. Kling, "Attosecond nanoscale near-field sampling," Nat. Commun. **7**, 11717 (2016).
4. M. G. Pullen, B. Wolter, A.-T. Le, M. Baudisch, M. Hemmer, A. Senftleben, C. D. Schröter, J. Ullrich, R. Moshammer, C. D. Lin, and J. Biegert, "Imaging an aligned polyatomic molecule with laser-induced electron diffraction," Nat. Commun. **6**(1), 7262 (2015).
5. M. Kübel, R. Siemering, C. Burger, N. G. Kling, H. Li, A. S. Alnaser, B. Bergues, S. Zherebtsov, A. M. Azzeer, I. Ben-Itzhak, R. Moshammer, R. de Vivie-Riedle, and M. F. Kling, "Steering proton migration in hydrocarbons using intense few-cycle laser fields," Phys. Rev. Lett. **116**(19), 193001 (2016).
6. B. Piglosiewicz, S. Schmidt, D. J. Park, J. Vogelsang, P. Groß, C. Manzoni, P. Farinello, G. Cerullo, and C. Lienau, "Carrier-envelope phase effects on the strong-field photoemission of electrons from metallic nanostructures," Nat. Photonics **8**(1), 37–42 (2014).
7. B. Wolter, M. G. Pullen, M. Baudisch, M. Sclafani, M. Hemmer, A. Senftleben, C. D. Schröter, J. Ullrich, R. Moshammer, and J. Biegert, "Strong-field physics with mid-IR fields," Phys. Rev. X **5**(2), 021034 (2015).
8. L. V. Keldysh, "Ionization in the field of a strong electromagnetic wave," Sov. Phys. JETP **20**, 1307–1314 (1964).
9. F. Silva, S. M. Teichmann, S. L. Cousin, M. Hemmer, and J. Biegert, "Spatiotemporal isolation of attosecond soft X-ray pulses in the water window," Nat. Commun. **6**(1), 6611 (2015).
10. Y. Pertot, C. Schmidt, M. Matthews, A. Chauvet, M. Huppert, V. Svoboda, A. von Conta, A. Tehlar, D. Baykusheva, J.-P. Wolf, and H. J. Wörner, "Time-resolved x-ray absorption spectroscopy with a water window high-harmonic source," Science **355**(6322), 264–267 (2017).

#327941 https://doi.org/10.1364/OE.26.016074
Journal © 2018 Received 9 Apr 2018; revised 16 May 2018; accepted 17 May 2018; published 11 Jun 2018

Optics EXPRESS

11. N. Thiré, R. Maksimenka, B. Kiss, C. Ferchaud, P. Bizouard, E. Cormier, K. Osvay, and N. Forget, "4-W, 100-kHz, few-cycle mid-infrared source with sub-100-mrad carrier-envelope phase noise," Opt. Express **25**(2), 1505–1514 (2017).
12. U. Elu, M. Baudisch, H. Pires, F. Tani, M. H. Frosz, F. Koettig, A. Ermolov, P. S. Russell, and J. Biegert, "High average power and single-cycle pulses from a mid-IR optical parametric chirped pulse amplifier," Optica **4**, 1024–1029 (2017).
13. M. Ueffing, S. Reiger, M. Kaumanns, V. Pervak, M. Trubetskov, T. Nubbemeyer, and F. Krausz, "Nonlinear pulse compression in a gas-filled multipass cell," Opt. Lett. **43**(9), 2070–2073 (2018).
14. H. Fattahi, H. G. Barros, M. Gorjan, T. Nubbemeyer, B. Alsaif, C. Y. Teisset, M. Schultze, S. Prinz, M. Haefner, M. Ueffing, A. Alismail, L. Vámos, A. Schwarz, O. Pronin, J. Brons, X. T. Geng, G. Arisholm, M. Ciappina, V. S. Yakovlev, D.-E. Kim, A. M. Azzeer, N. Karpowicz, D. Sutter, Z. Major, T. Metzger, and F. Krausz, "Third-generation femtosecond technology," Optica **1**(1), 45–63 (2014).
15. C. Homann, M. Bradler, M. Förster, P. Hommelhoff, and E. Riedle, "Carrier-envelope phase stable sub-two-cycle pulses tunable around 1.8 µm at 100 kHz," Opt. Lett. **37**(10), 1673–1675 (2012).
16. B. E. Schmidt, A. Hage, T. Mans, F. Légaré, and H.-J. Wörner, "Highly stable, 54mJ Yb-InnoSlab laser platform at 0.5kW average power," Opt. Express **25**(15), 17549–17555 (2017).
17. T. Metzger, A. Schwarz, C. Y. Teisset, D. Sutter, A. Killi, R. Kienberger, and F. Krausz, "High-repetition-rate picosecond pump laser based on a Yb:YAG disk amplifier for optical parametric amplification," Opt. Lett. **34**(14), 2123–2125 (2009).
18. P. Russbueldt, T. Mans, G. Rotarius, J. Weitenberg, H. D. Hoffmann, and R. Poprawe, "400W Yb:YAG Innoslab fs-Amplifier," Opt. Express **17**(15), 12230–12245 (2009).
19. M. Müller, M. Kienel, A. Klenke, T. Gottschall, E. Shestaev, M. Plötner, J. Limpert, and A. Tünnermann, "1 kW 1 mJ eight-channel ultrafast fiber laser," Opt. Lett. **41**(15), 3439–3442 (2016).
20. M. Bradler, C. Homann, and E. Riedle, "Broadband difference frequency mixing between visible and near-infrared pulses for few-cycle pulse generation with stable carrier-envelope phase," Appl. Phys. B **113**(1), 19–25 (2013).
21. M. Bradler, P. Baum, and E. Riedle, "Femtosecond continuum generation in bulk laser host materials with sub-µJ pump pulses," Appl. Phys. B **97**(3), 561–574 (2009).
22. A. L. Calendron, H. Çankaya, G. Cirmi, and F. X. Kärtner, "White-light generation with sub-ps pulses," Opt. Express **23**(11), 13866–13879 (2015).
23. J. Galinis, G. Tamošauskas, I. Gražulevičiūtė, E. Keblytė, V. Jukna, and A. Dubietis, "Filamentation and supercontinuum generation in solid-state dielectric media with picosecond laser pulses," Phys. Rev. A **92**(3), 033857 (2015).
24. M. Bradler, L. Kasmi, P. Baum, and E. Riedle, "Pushing the NOPA to New Frontiers: Output to Below 400 nm, MHz Operation and ps Pump Duration," in *Ultrafast Phenomena XIX* (Springer Int. Pub. 2014), pp. 757–760.
25. H. Fattahi, H. Wang, A. Alismail, G. Arisholm, V. Pervak, A. M. Azzeer, and F. Krausz, "Near-PHz-bandwidth, phase-stable continua generated from a Yb:YAG thin-disk amplifier," Opt. Express **24**(21), 24337–24346 (2016).
26. M. Kolesik, G. Katona, J. V. Moloney, and E. M. Wright, "Theory and simulation of supercontinuum generation in transparent bulk media," Appl. Phys. B **77**(2-3), 185–195 (2003).
27. J. Lee Rodgers and W. A. Nicewander, "Thirteen ways to look at the correlation coefficient," Am. Stat. **42**(1), 59–66 (1988).
28. P. Wnuk, H. Fuest, M. Neuhaus, L. Loetscher, S. Zherebtsov, E. Riedle, Z. Major, and M. F. Kling, "Discrete dispersion scanning as a simple method for broadband femtosecond pulse characterization," Opt. Express **24**(16), 18551–18558 (2016).
29. M. Kakehata, H. Takada, Y. Kobayashi, K. Torizuka, Y. Fujihira, T. Homma, and H. Takahashi, "Single-shot measurement of carrier-envelope phase changes by spectral interferometry," Opt. Lett. **26**(18), 1436–1438 (2001).
30. A. Thai, M. Hemmer, P. K. Bates, O. Chalus, and J. Biegert, "Sub-250-mrad, passively carrier-envelope-phase-stable mid-infrared OPCPA source at high repetition rate," Opt. Lett. **36**(19), 3918–3920 (2011).
31. C. Li, E. Moon, H. Wang, H. Mashiko, C. M. Nakamura, J. Tackett, and Z. Chang, "Determining the phase-energy coupling coefficient in carrier-envelope phase measurements," Opt. Lett. **32**(7), 796–798 (2007).
32. T. Stanislauskas, R. Antipenkov, V. Martinenaite, L. Karpavcius, A. Varanavicius, V. Sinkevicius, P. Miseikis, D. Grigaitis, and T. Balciunas, "Carrier-envelope phase control of Yb:KGW laser and parametric amplifiers," CLEO EUROPE/EQEC, 12–16 May 2013.
33. C. Burger, W. F. Frisch, T. M. Kardaś, M. Trubetskov, V. Pervak, R. Moshammer, B. Bergues, M. F. Kling, and P. Wnuk, "Compact and flexible harmonic generator and three-color synthesizer for femtosecond coherent control and time-resolved studies," Opt. Express **25**(25), 31130–31139 (2017).
34. M. Ueffing, R. Lange, T. Pleyer, V. Pervak, T. Metzger, D. Sutter, Z. Major, T. Nubbemeyer, and F. Krausz, "Direct regenerative amplification of femtosecond pulses to the multimillijoule level," Opt. Lett. **41**(16), 3840–3843 (2016).
35. T. Nubbemeyer, M. Kaumanns, M. Ueffing, M. Gorjan, A. Alismail, H. Fattahi, J. Brons, O. Pronin, H. G. Barros, Z. Major, T. Metzger, D. Sutter, and F. Krausz, "Powerful 100-fs-scale Kerr-lens mode-locked thin-disk oscillator," Opt. Lett. **42**, 1381–1384 (2017).

Optics EXPRESS

1. Introduction

Owing to their short pulse duration, femtosecond sources are indispensable for studying and controlling ultrafast chemical transformations [1] and uncovering the realms of strong field physics in atoms, molecules, solids [2] and nanoscale targets [3]. In particular, intense mid-infrared laser systems (2-5 μm) have recently been applied in imaging molecular structure via laser-induced electron diffraction [4], opening the door towards 4D-imaging with highest possible temporal and spatial resolutions. In all these cases, strong-field driven processes rely on precise control of the electrical field waveform under the pulse envelope. For few-cycle pulses such control can be achieved by carrier-envelope phase (CEP) stabilization.

Numerous studies on steering strong-field processes with the CEP have been performed [5,6], most of them, however, with Ti:sapphire laser systems operating around 800 nm. While studies in the mid-infrared are still scarce [7], they gain importance in strong-field experiments due to the λ^2 scaling of the cut-off energies of ionized electrons accelerated by the ponderomotive force and of the cut-off in high harmonic generation [8]. This has recently permitted the generation of water-window attosecond soft x-ray pulses [9] and their application in molecular spectroscopy [10]. This scaling, however, is somewhat limited by the pulse duration. At around 2 μm, sub-three-cycle pulses are commonly achieved, whereas this becomes significantly more difficult for longer wavelength [11]. Additionally, the likelihood of strong-field processes, such as electron recollision, is strongly reduced with longer wavelengths. Moreover, as strong field experiments are often carried out in diluted media (e.g. low-pressure gases), high repetition rate sources are necessary to overcome the associated low signal generated from single pulse excitation. Recent results demonstrate feasibility of obtaining a 60 μJ CEP-stable source at 160 kHz repetition rate [12] through parametric amplification. A novel approach, based on spectral broadening in noble gases of a high average power Ytterbium-doped amplifier with compression down to 35 fs [13], paves the road for high-average-power CEP-stable sources.

At high repetition rates, 3rd-generation femtosecond sources [14] relying on optical parametric (chirped pulse) amplification (OPA/OPCPA) offer favorable power scaling, as the parametric processes involved in principle do not deposit heat in the nonlinear crystals except for small residual material absorption. Additionally, difference frequency generation (DFG) used for generation of mid-infrared beams implies passive CEP stabilization, as the CEP between both interacting beams cancels out.

Here, we follow an approach to generate CEP-stable few-cycle pulses first demonstrated by Homann *et al*. [15]. This scheme relies on self-seeding with bulk supercontinuum generation produced by the main pump laser and therefore requires no active temporal synchronization between pump and seed laser. For Homann *et al*. the use of a sub-ps laser led to a restriction of available pump-laser output power [15]. High average power pump lasers generally come at the cost of narrower bandwidth with typically picosecond pulse durations. Recently, it has been shown by Schmidt *et al*. [16] that an Innoslab amplifier can be used to generate two-cycle mid-infrared seed pulses. In this work, we use an Innoslab-based laser system for the self-seeded generation of CEP-stable 2 μm pulses, which are subsequently amplified to 100 μJ levels at 100 kHz repetition rate.

2. Layout of the few-cycle mid-infrared source

For high average power (sub-)picosecond laser sources, two competing technologies are available: disk amplifiers [17], and Innoslab amplifiers [18]. Both technologies are based on Ytterbium-doped Yttrium aluminium garnet (Yb:YAG), delivering pulses around 1030 nm with average powers reaching into the kW range. Just recently large mode area fibers [19] could reach similar parameters. Innoslab technology offers the advantage that due to the higher gain the B-integral in the crystal as well as the beam path length can be reduced leading to a good stability of the system. In our laser architecture, the seed pulses for the amplifiers were delivered by an Yb-doped fused silica fiber oscillator (Active Fiber Systems),

Optics EXPRESS

centered at 1030 nm. The pulses were stretched up to 1.5 ns in a single grating Martinez-type stretcher. Afterwards, they were preamplified to 1.2 µJ in a fiber amplifier (Active Fiber Systems). Final amplification was achieved in an Innoslab amplifier (built at ILT Aachen), capable of delivering up to 400 W at a repetition rate of 0.1-1 MHz before compression. In the work presented here, we used a repetition rate of 100 kHz and uncompressed output powers of 170 W. The amplified 1030 nm pulses were compressed to 1.1 ps in a transmission grating compressor (single grating Treacy configuration) with 66% efficiency (110 W).

Due to the enclosed construction of the pump laser chain and internal beam stabilization as well as a beam pointing stabilization behind the compressor, hands-off operation of the pump laser with good day-to-day operation stability was achieved. This aspect is especially important for pumping parametric amplifiers, which are sensitive to both beam pointing and energy variations. In our case this allowed the full setup to be brought to previous day condition in less than 10 min. The scheme for the entire mid-infrared laser system is shown in Fig. 1.

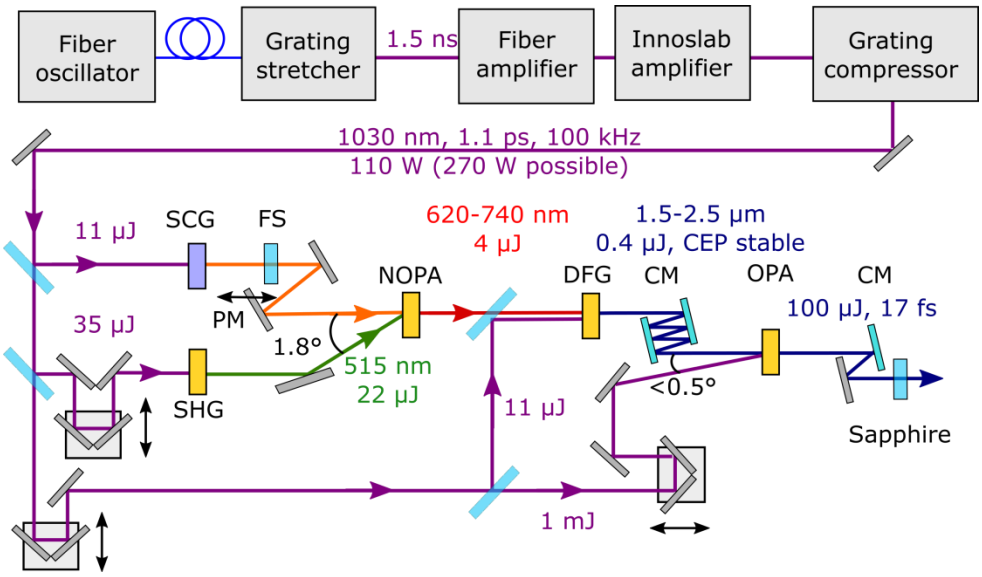

Fig. 1. Sketch of the mid-infrared laser system; SCG: supercontinuum generation, SHG: second harmonic generation, FS: fused silica, CM: chirped mirrors, PM: piezo mirror.

The generation of the CEP-stable mid-IR seed (to be later amplified in an OPA), is similar to previous work [15,20]. The pump light is split into four independent channels. The first part is used for supercontinuum generation, the second is frequency doubled and used as a pump for a non-collinear optical parametric amplifier (NOPA), which amplifies the red part (620-740 nm) of the supercontinuum. The amplified beam serves as a pump beam in a DFG process, where it is collinearly mixed with the third part of the 1030 nm beam, generating the passively CEP-stable mid-IR idler beam. This mid-IR beam is then amplified in an OPA stage pumped by the main part of the pump laser power. The calculations of the small signal gain (without spatial effects such as: diffraction, walk-off and temporal effects: temporal walk-off, spectral phase, saturation effects) has been performed to analyze conversion bandwidths of the consecutive nonlinear stages (NOPA, DFG, OPA). As can be seen in Fig. 2(a), the small signal gain profiles overlap for NOPA, DFG and OPA. The limiting factor is the bandwidth of the OPA, which is shown in Fig. 2(b) for beta-barium borate (BBO), bismuth triborate (BiBO), lithium niobate (LNB), and lithium triborate (LBO). Compression of the pulses was accomplished by a combination of chirped mirrors (CM) and bulk material as will be discussed later.

Optics EXPRESS

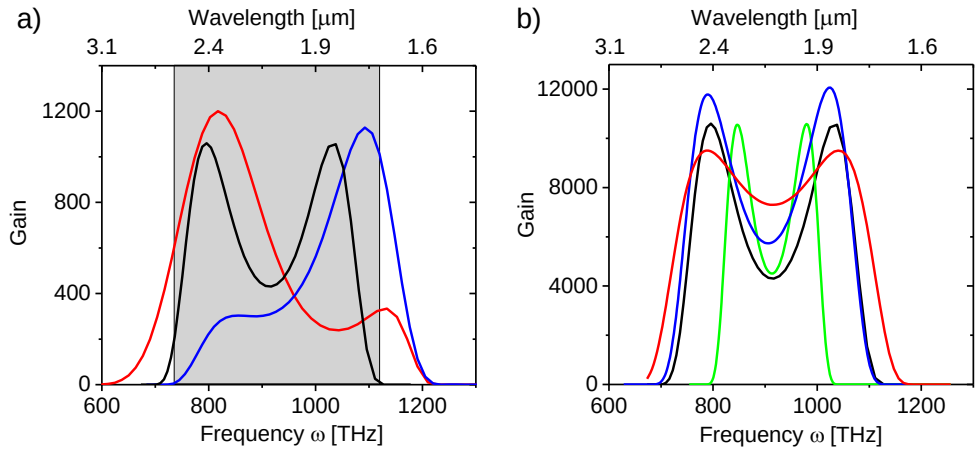

Fig. 2. Calculated small gain profiles: a) NOPA (red), DFG (blue) and OPA (black) processes: The NOPA spectrum is frequency down-shifted corresponding to 1030 nm for easier comparison. The shaded area marks the spectral overlap of all three bands (type-I phase matching profiles in BBO for NOPA and DFG and in BiBO for the OPA). b) Amplification curves calculated for the OPA stage for four different nonlinear crystals: BiBO (black), BBO (blue), LNB (red), and LBO (green).

3. Results

3.1 Supercontinuum generation

To seed the NOPA with a spectral bandwidth supporting ultrashort pulses, the narrowband (2 nm FWHM) pump pulses needed first to be significantly broadened. Supercontinuum generation (SCG) in a bulk material, like sapphire or YAG is a commonly used technique in the femtosecond regime [21,22]. When the pulse duration increases to the picosecond range, the power needed for significant broadening approaches the damage threshold of the material making the generation of supercontinua more challenging. Although SCG with picosecond pulses has recently been achieved [22–24], its properties are still less studied than in the femtosecond range, and application in CEP stable sources is scarce [11].

To establish optimal conditions for SCG we tested two commonly used materials, YAG and sapphire. For our experimental conditions, only YAG provided stable generation conditions. In sapphire the SC covers mostly the range from 500 to 600 nm with an order of magnitude less intensity in the region of interest compared to YAG, and was extremely prone to damage. For the optimal case in YAG, the filament visible as white glow through the side of the crystal, as seen in Fig. 3(b), started around 1 mm behind the input face with a length of 4.5 mm. Accordingly, a 6 mm long crystal was used. Stable SC could be achieved with fundamental pulse energies in the range of 8-15 μJ depending on the focusing lens and crystal position relative to the focus. In our case, the most stable results for white light generation could be achieved for an input energy of 11 μJ focused with a f = 75 mm lens to a diameter of around 20 μm. A typical spectrum of such broadened light, together with its spatial profile is shown in Fig. 3(a). The crystal did not have to be continuously moved. Occasionally (50-100 operation hours) a sudden deterioration of the filament was observed, which was solved by small translation of the crystal. We also noticed, using a thermographic camera, that the temperature of the YAG crystal increased slightly over the first few minutes, leading to 5-7 °C temperature rise with respect to ambient temperature, cf. Figure 3(c), indicating some residual absorption of the pump beam, most likely by avalanche ionization or multiphoton absorption.

Optics EXPRESS

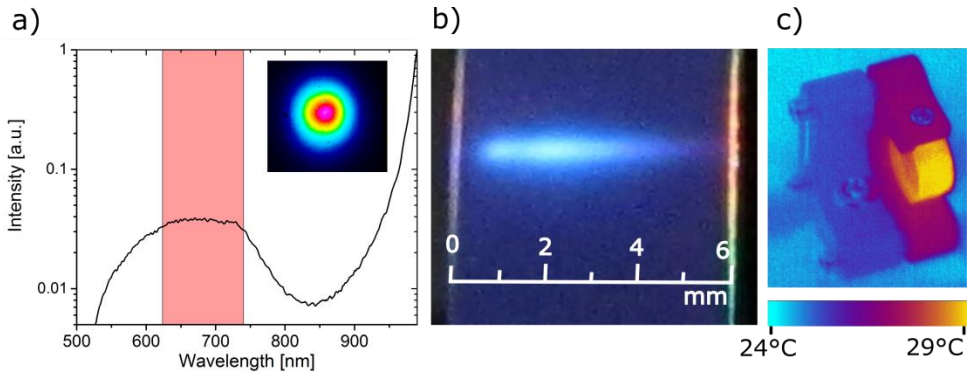

Fig. 3. a) Spectrum of the supercontinuum generated with 1.1 ps pulses centered at 1030 nm in a 6 mm YAG crystal. The colored area marks the spectral bandwidth of the successive NOPA stage. The inset shows the spatial profile of the generated supercontinuum. b) Picture of the filament through the side of the crystal. c) Thermal image of the YAG crystal during SC generation.

For optimal conditions, the position of the YAG crystal needed to be carefully adjusted, corresponding to a position approximately 1 mm behind the focus. This was important to avoid multiple filamentation, visible by eye as two subsequent filaments through the side of the crystal or by spectral modulations. Furthermore, the focus position was also crucial, within few tens of μm, for output stability, in particular with respect to CEP fluctuations. After placing the crystal, the output spectrum was stable without need of motion of the crystal to avoid damage. While it is often believed that supercontinua generated with picosecond pulses are not stable enough, especially to be used directly as a seed for a system with passive CEP stabilization [25], here, we could confirm that this is not the case. A train of supercontinuum pulses was recorded with a photodiode behind a bandpass filter transmitting a band of 40 nm centered around 700 nm. This closely corresponds to the central band of the following NOPA amplifier. Figure 4(a) shows a histogram of the energy distribution of the generated light. As can be seen, the generated SC is highly stable with a distribution width below 0.9% but with an asymmetric energy distribution. This indicates intensity clamping, which is expected for supercontinuum generation [26], limiting the energy of the generated white light. It was further confirmed as increasing the energy of the driving pulse (and readjusting the focusing condition) did not lead to an increase of the spectral density of the SC. To investigate the temporal correlation between pulses the Pearson correlation was evaluated [27]:

$$\gamma_{E,E+j} = \frac{\sum_{i=1}^{N}(E_i - \bar{E})\cdot(\mathrm{E}_{i+j} - \bar{\mathrm{E}})}{\sum_{i=1}^{N}(\mathrm{E}_i - \bar{\mathrm{E}})^2}, \qquad (1)$$

where E_i and $\bar{E}$ are pulse energy and its average value, respectively, and N is the number of pulses. As can be seen in Fig. 4(b), there is only 27% correlation between two consecutive shots and almost no correlation for further separated pulses. This proves that the source has similar characteristic as white noise, and thus its stability should improve with pulse averaging, as shown in Fig. 4(c). This, together with the small value of the rms noise, promises good stability of the CEP.

Optics EXPRESS

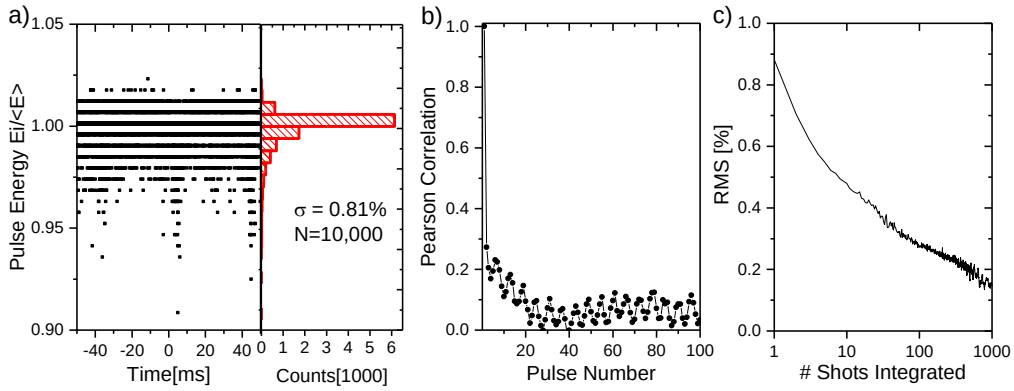

Fig. 4. Noise characteristic of the generated supercontinuum; a) Pulse energy fluctuation of consecutive pulses with power histogram b) Pearson correlation; c) Rms value for different number of accumulated shots.

3.2 Mid-IR pulse generation and amplification

The second part of the fundamental beam was frequency doubled in a 2 mm BBO crystal at an intensity of 60 GW/cm^2 (similar intensities were used in the following nonlinear processes). We obtained 22 μJ at 515 nm with a conversion efficiency of 63%. The generated second harmonic beam was then used as a pump for the SC-seeded NOPA to amplify a spectral range of 620-740 nm. A 4-mm thick BBO crystal was used with phase-matching angle of θ = 23.3° and a noncollinearity angle of 1.8° between pump and signal. As can be seen in Fig. 5(a), the bandwidth of the amplified pulses (black line) corresponds well to the calculated small gain profile (red line). The discrepancy between the spectra could be due to the simplified model used in the calculation, not including spatial properties of the supercontinuum (different spectral components have different divergence) and its spectral chirp. The spectral chirp of the supercontinuum (mostly due to material dispersion), beside a quadratic term, possesses a significant third order term. This causes smaller temporal stretching of the longer wavelengths part of the SC as compared to short wavelengths. This, together with the saturation effects in the NOPA, could lead to lower extraction of the pump energy of the less chirped (i.e. long wavelength) part of the spectrum, explaining the observed discrepancy.

To increase the final power of the mid-IR output, an additional NOPA amplification stage could be added before the DFG stage. However, this would increase the overall path length of the pump and seed arm before DFG, where any length variations between two arms would directly transfer into CEP fluctuations. We therefore decided for DFG immediately after the single-stage NOPA and post-amplification of the mid-IR pulses. For DFG we used a 1 mm BBO crystal cut at 21.5°. The seed (1030 nm, 11 μJ) and pump (NOPA output) where collinearly combined with a dichroic mirror to avoid angular chirp of the generated mid-IR idler beam. As a result, CEP-stable mid-IR pulses were generated with energies of 0.4 μJ and bandwidths covering a range of 1.5-2.5 μm (see Fig. 5(b)). The spectrum closely resembles the theoretical gain curve.

Optics EXPRESS

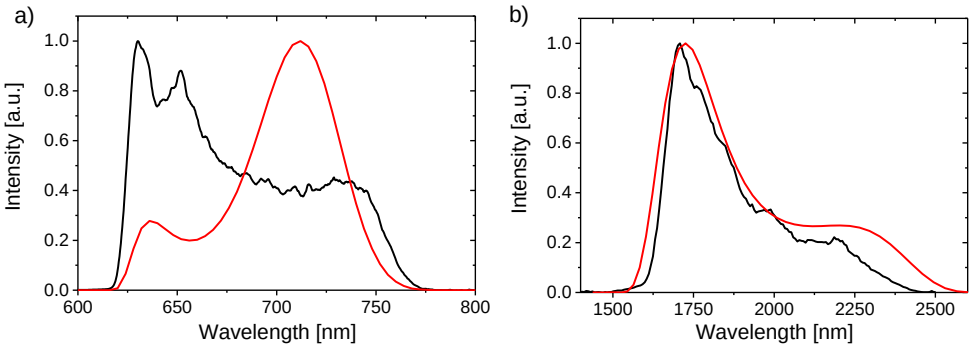

Fig. 5. Spectra of a) the NOPA and b) DFG output pulses. Black lines: measured spectra, red lines: calculated small signal gain profiles.

3.3 Mid-IR pulse amplification

The mid-IR beam was amplified in an OPA stage pumped by the 1030 nm beam with 1 mJ energy. In order to separate signal and idler after amplification, as they spectrally overlap and have the same polarization, pump and seed needed to be aligned under an angle of about 0.5°. The high gain and therefore high average pump power required to reach amplification in a single stage led to various challenges, which we discuss in the following. In our experiments, three different nonlinear crystals where tested: BBO, LNB and BiBO.

First, a 4 mm thick BBO was tested. Using this crystal, up to 120 µJ of output energy could be achieved in the mid-IR. However, the crystal was heated by more than 100 °C, which we associated with absorption of the idler beam (with pump beam only the temperature rise of the crystal was only negligible). This led to thermal stress in the crystal, which made it very prone to shattering. Most of the heating inside of the BBO crystal occurred close to the output surface where due to the exponential nature of the amplification a significant portion of the idler was generated. Simulations using a finite element method indicated that the thermally induced stress for the same temperature gradient in a 1 mm thick crystal is two times smaller than for a 4 mm thick crystal. For that reason, we tried splitting the 4 mm crystal into two thinner ones with thickness of 3 mm followed by a 1 mm BBO so that the thermal load was mostly located in the thinner crystal. Crystals were placed within a distance of less than 1 cm to keep the spatial beam separation, caused by the nonlinear angle, smaller than the beam size. Although this approach avoided crystal cracking, still the high temperature of the second crystal as well as the spatial separation between beams lead to an unfavorable beam profile as well as pointing fluctuations.

In the second attempt a LNB-crystal was tested in the OPA stage. With crystal thickness of 4 mm the pump intensity had to be reduced to below 50 GW/cm^2. Higher intensities led to deterioration of the beam by the photorefractive effect which eventually could lead to a runaway focusing process damaging the crystal. Even below critical focusing, this effect led to a slow thermalization and power stabilization on the time scale of hours. In this configuration, the average output power was limited to 8 W, but with a broader spectrum than for BBO as can be seen in Fig. 6(b).

In the final configuration, we used a 4 mm thick BiBO crystal, cut in the XY-plane. Output pulse energies of 100 µJ could be achieved. Due to impurities in the crystal, its temperature was elevated by 30°C by the pump beam alone. Adding the seed beam and thereby amplification lead only to a small additional temperature increase of less than 5°C. This change in temperature influenced the phase matching in the crystal. As the crystal thermalized after a few minutes, this, however, was not problematic. Due to the lower heating compared to BBO as well as more stable output conditions compared to LNB and reasonable output power, we concluded that this configuration is most favorable.

Optics EXPRESS

The output pulse spectrum is only slightly narrower at short wavelengths as compared to the DFG output, as is expected from the theoretical gain curves in Fig. 2(a), but still broad enough to support few-cycle pulses. The high energy-stability of the OPA amplifier was achieved by saturation. This minimizes energy coupling of the previous stages to the final energy. As a result, the final stability of the mid-IR pulses was at a level below 0.9% rms, only slightly higher than the noise of the pump laser with 0.6% rms.

3.4 Pulse compression and CEP stability

In order to compress the pulses their chirp first needed to be characterized. We were faced with the challenge that the signal for second-harmonic generation frequency-resolved optical gating (SHG-FROG) is in the range of 800-1250 nm, where no single spectrometer is available, and the intensity of the uncompressed pulses was too low for higher order nonlinear characterization techniques, e.g. third-harmonic generation FROG. To overcome these limitations we used a technique based on discrete dispersion scanning. It allows characterization of strongly chirped pulses with high sensitivity, using only dispersive material, a nonlinear crystal, and a spectrometer [28]. Based on this information we could properly design the chirped pulse compressor.

Most of the standard dispersive materials have positive group delay dispersion (GDD) in the visible and negative GDD in the mid-IR, allowing, in theory, simple material compression. Unfortunately, for such broadband pulses, the third order dispersion (TOD) becomes important, which is positive for materials in both spectral ranges. Therefore, additional custom-made chirped mirrors were designed to introduce negative TOD (see Fig. 6(c)).

For optimal amplification, especially in the last OPA stage, the duration of the seed needed to be stretched enough to ensure temporal overlap with the 1.1 ps long pump pulse. As can be seen in Fig. 1, 15 mm of fused silica were placed in the visible beam after SCG for the above reported results. Additionally 6 bounces off the chirped mirrors were used in the mid-IR beam before OPA. To compress the pulses after amplification only one bounce off a chirped mirror and about 25 mm of transparent material (20 mm sapphire, due to a low TOD/GDD ratio and about 5 mm functional elements used for the FROG) were used. By adjusting the amount of material before and after amplification as well as the number of chirped mirror bounces, the temporal overlap in all parametric stages can be flexibly adjusted well as final pulse compression with a reliable and stable compressor throughput of over 85% can be achieved.

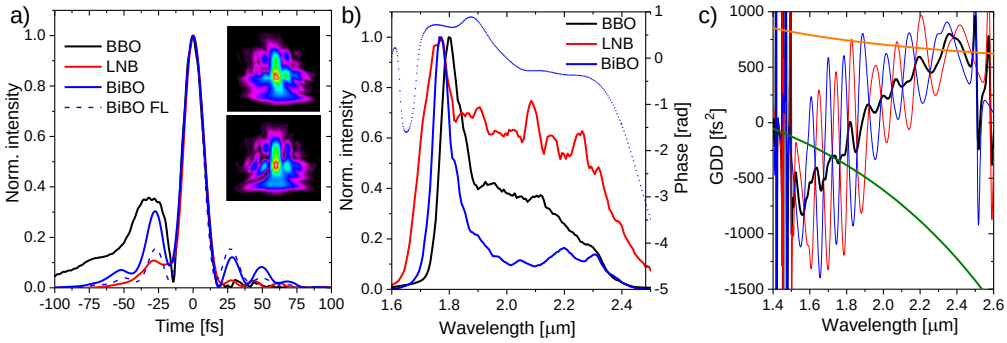

Fig. 6. Temporal characterization of the mid-IR pulses with THG-FROG; a) retrieved temporal profile for different crystals and calculated Fourier-limited pulse (dashed line) for BiBO, inset: measured (upper) and retrieved (lower) FROG traces for BiBO. b) Measured spectra for all amplification crystals with retrieved phase. c) GDD introduced by 1 chirped mirror (design curve, red at 5°, blue at 23° AOI, black – average value), by 5 mm of sapphire (green) and GDD introduced in the mid-IR beam by placing 15 mm of UV fused silica in the supercontinuum output (orange).

Optics EXPRESS

The compressed pulses were characterized with a THG-FROG measurement (see Fig. 6). The retrieved pulse duration for BiBO was 17.1 fs FWHM (blue line in Fig. 6(a)), which corresponds to 2.7 optical cycles. Similar durations were retrieved for BBO with 17.3 fs and for LNB with 16.3 fs. The duration of the compressed pulse for BiBO is almost identical to the Fourier limited case, with 66% of the pulse energy contained in the main pulse for BiBO, 85% for LNB and 51% for BBO. The only differences are modified heights of the pre- and post-pulses. The modulated temporal structure is a result of the uneven shape of the amplified spectrum, visible in Fig. 6(b), as well as phase ripples from the chirped mirrors, which may be improved with revised CM designs in the future.

To measure the stability of the CEP we used a home-built f-2f interferometer in collinear geometry [29]. As the spectrum of the pulses is less than octave spanning, they needed to be spectrally broadened, which was achieved through SC generation in a sapphire crystal using pulses with an energy of 2 μJ. Spectral interference fringes were recorded with a compact spectrometer, operating at a frequency of up to 80 Hz and an acquisition time of 4 ms. Time traces for the passively CEP-stabilized pulses are shown in Fig. 7.

We observed slow drifts on timescales of several seconds that were most likely due to the interferometric nature of the DFG process. To compensate such slow drifts, we implemented a piezo-driven mirror in the white light beam path before the DFG stage. This allows rapid and fine tuning of the CEP phase of the generated mid-IR pulses [30]. This way, the rms value of the CEP was measured to be 242 mrad over a time period of 30 min (in-loop measurement). We note here that high contrast of the measured CEP fringes implies that, although spectra were integrated over 400 laser shots, their relative CEP had similar values.

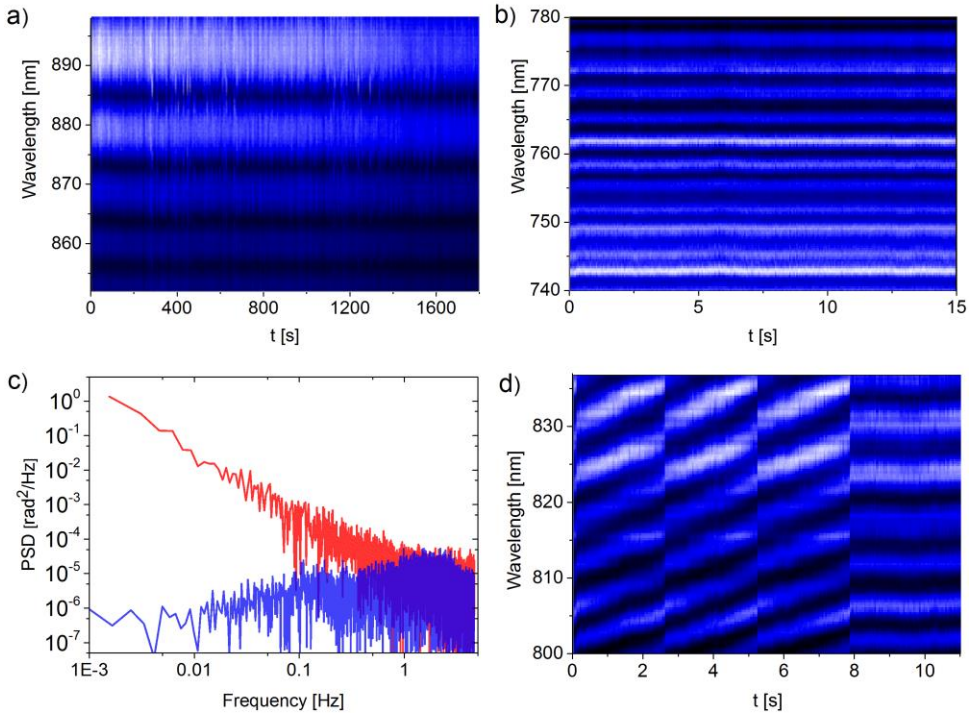

Fig. 7. CEP phase stability: a) Interference fringes recorded with feedback-loop recorded for 30 min with 242 mrad fluctuations b) For lower amplification,15 s without feedback-loop with 103 mrad fluctuations, c) comparison of the CEP noise (power spectral density) with (blue) and without (red) stabilization and d) example of the CEP phase control (0-π ramp pattern, followed by constant CEP).

Optics EXPRESS

It was observed that most of these fluctuations are caused by overcompensation of the beam pointing stabilization placed behind the grating compressor that was necessary to avoid thermally induced drifts. Other causes are thermal fluctuations in either the OPA crystal, air, or optical elements. This could be seen, as reducing the laser pump power to about 27 W and reducing OPA pump power to 13% (and keeping the intensity in the OPA similar by adjusting the beam sizes) lower fluctuations of 136 mrad were observed over 20 minutes. Without piezo mirror stabilization, 103 mrad fluctuations over 15 seconds were measured. Some of these fluctuations might be measurement artefacts as fluctuations in laser power and beam pointing can couple to the measured CEP [31,32] due to position variations of the filament in SCG in the f-2f interferometer.

Besides slow phase corrections, the piezo driven mirror allowed us to introduce fast CEP control (see Fig. 7(d)). Thanks to the low weight of the mirror and a high strength piezo actuator the temporal response of the system was faster than the temporal resolution of our f-2f setup (12.5 ms). This offers a faster response time than approaches based on wedge scanning or translation of a grating and could be used for fast CEP corrections or experiments where rapid CEP scanning is necessary.

4. Conclusions

We could demonstrate the generation of highly stable, few-cycle mid-IR pulses with 100 μJ of output energy at 100 kHz repetition rate utilizing 110 W compressed pulses from a fiber-laser seeded Innoslab amplifier. With these parameters the system currently provides the highest average power with few-cycle pulse duration in the mid-IR. We could show that the picosecond driving pulses are sufficient for generation of stable, low noise supercontinuum in a bulk YAG crystal supporting highly CEP-stable pulses. We compared the limiting factors in the three most suitable crystals for further amplification of a DFG-generated mid-IR pulse: BBO, LNB and BiBO with regards to high gain amplification in a single OPA stage. All crystals give similar output parameters. However, BiBO provided the best compromise between output power and overall stability. The presented approach is well scalable. The limiting factor, which for BiBO case is the moderate crystal heating, could be overcome either by providing a high quality (low impurities) large aperture BiBO crystal or by active cooling of the crystal. Higher output energies would be achievable by increasing the pump power and beam size in the OPA.

The dispersion control was achieved in a hybrid material - chirped mirror setup leading to compression to around 17 fs, which corresponds to 2.7 oscillations of the electric field. This compression method offers good flexibility without the need of an acousto-optic programmable dispersive filter (AOPDF), which is currently not commercially available as a standalone device at 100 kHz. The CEP stability was around 240 mrad for over 30 min.

As the Innoslab amplifier can provide additional 1.6 mJ of compressed pulse energy, the system offers the ability to further amplify the mid-IR pulses in the same amplification stage or with an additional stage. This additional power could also be used to generate pulses at different wavelength for multicolor experiments [14,33]. Our approach will benefit from the recent and ongoing advances of high average power pump laser sources and their improved availability [18,34,35].

In summary, we could show a simple and cost efficient approach to reach unprecedented average power CEP-stable mid-IR radiation. The unique parameters of the system permit, amongst others, studying strong field phenomena in gases and solid media at high acquisition rates.

Funding

Max Planck Society, the German Research Foundation (DFG) via LMUexcellent and the cluster of excellence “Munich Centre for Advanced Photonics (MAP)”, the BMBF via NEXUS (13N12080), and the European Union (EU) via the ERC grant ATTOCO. P.W.

Optics EXPRESS

acknowledges a Mobility Plus fellowship (no. 1283/MOB/IV/2015/0) from the Polish Ministry of Science and Higher Education.

Acknowledgments

We acknowledge support from and fruitful discussions with P. Baum, Y. Deng, R. Ernstorfer, H. Fattahi, F. Krausz, and J. Weitenberg.